ACS OMEGA

http://pubs.acs.org/journal/acsodf

Article

Silicone-Based Multifunctional Thin Films with Improved Triboelectric and Sensing Performances via Chemically Interfacial Modification

Habtamu Gebeyehu Menge, Min Woo Kim, Sangmin Lee,* and Yong Tae Park*

Cite This: *ACS Omega* 2023, 8, 7135−7142

Read Online

ACCESS | Metrics & More | Article Recommendations | Supporting Information

ABSTRACT: The development of triboelectric nanogenerators (TENGs) technology has advanced in recent years. However, TENG performance is affected by the screened-out surface charge density owing to the abundant free electrons and physical adhesion at the electrode-tribomaterial interface. Furthermore, the demand for flexible and soft electrodes is higher than that for stiff electrodes for patchable nanogenerators. This study introduces a chemically cross-linked (XL) graphene-based electrode with a silicone elastomer using hydrolyzed 3-aminopropylenetriethoxysilanes. The conductive graphene-based multilayered electrode was successfully assembled on a modified silicone elastomer using a cheap and eco-friendly layer-by-layer assembly method. As a proof-of-concept, the droplet-driven TENG with the chemically XL electrode of silicone elastomer exhibited an output power of approximately 2-fold improvement owing to its higher surface charge density than without XL. This chemically XL electrode of silicone elastomer film demonstrated remarkable stability and resistance to repeated mechanical deformations like bending and stretching. Moreover, due to the chemical XL effects, it was used as a strain sensor to detect subtle motions and exhibited high sensitivity. Thus, this cheap, convenient, and sustainable design approach can provide a platform for future multifunctional wearable electronic devices.

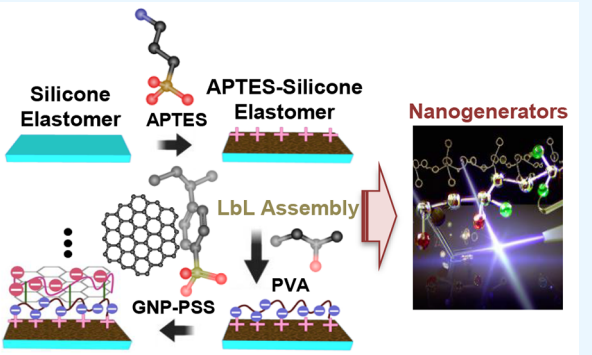

INTRODUCTION

Technology is considerably improving the quality of our lives through portable and wearable technological gadgets.[1] In this regard, triboelectric nanogenerators (TENGs) have sparked much attention as new mechanical energy scavenger that generates electricity.[2,3] TENGs have been successfully shown in various applications with advantages such as high electrical output power, high material selection, lightweight, and great adaptability to varied applications.[4−7]

Despite the success of using a variety of coating processes to create TENG devices,[8−11] challenges still need to be solved before these approaches can be commercialized, including the cost of tribomaterial (TM) fabrications and sustainable power sources.[12−15] Furthermore, as stated in previous reports,[16,17] several approaches have been tried to improve the performance of TENGs. However, the surface charge density screened out still needs to be solved, caused by factors such as an abundance of free interfacial electrons[16,18,19] and physical adhesion at the electrode−TM interface. Particularly, the latter still needs to be taken into account. As a result, the electrical stability and conductivity of electrodes adhering to TMs was impaired, affecting TENG performances. In addition, attachable wearable electronic devices require the substitution of stiff electrodes with soft and stretchable elastomeric electrodes because elastomeric films can withstand repeated mechanical deformations such as bending, twisting, and stretching.[20−23]

This study introduces chemically cross-linked (XL) electrodes with silicone elastomer films (polydimethylsiloxane (PDMS) and dragon skin (DS)) to preserve the surface charge density and improve the TENG and sensitivity performances. We considered silicone elastomeric films because of their high flexibility, softness, optical transparency, biocompatibility, and ease of fabrication.[23,24] However, the hydrophobicity and the low surface energy of silicone elastomers made it difficult to interact with other species. Various methods, such as chemical and energy manipulation, have been developed to manipulate the surface energy of silicone elastomers.[24−28] Here, we presented a quick and easy method for surface modification by one-time dipping in a hydrolyzed 3-aminopropylenetriethoxysilanes (APTES) solution at room temperature. The chemical interaction between

Received: January 1, 2023
Accepted: January 31, 2023
Published: February 10, 2023

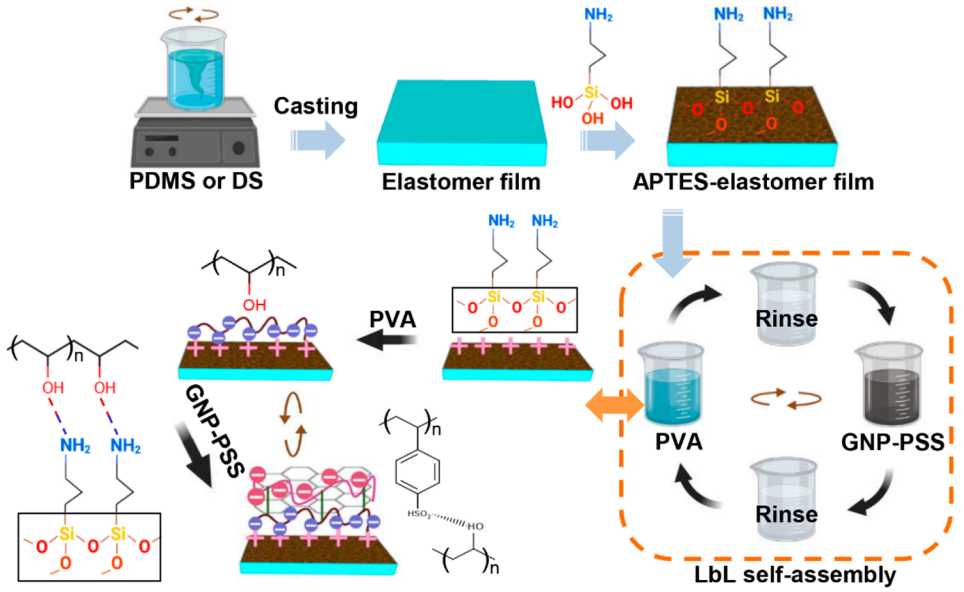

Figure 1. Schematic illustration of chemically cross-linked conductive silicone elastomer film fabrication.

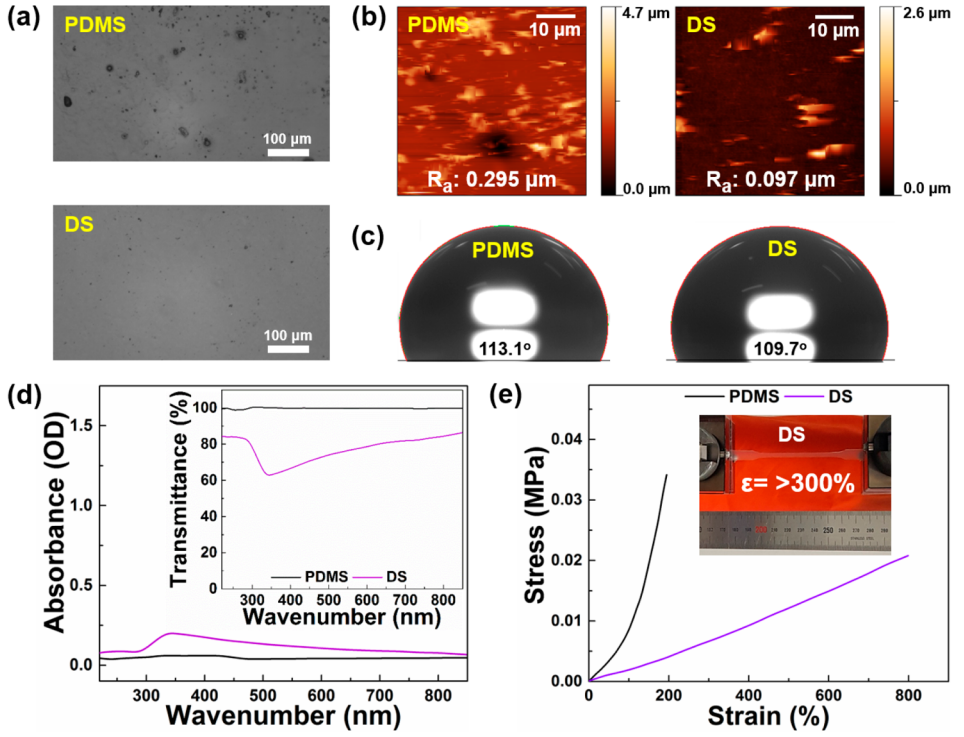

Figure 2. (a) Optical microscopic images of PDMS and DS films, (b) 2D AFM surface morphologies of PDMS and DS films, (c) water contact angles of PDMS and DS films at room temperature, (d) UV−vis light absorbance spectra of PDMS and DS films (the inset is the UV−vis light transmittance spectra of PDMS and DS films), and (e) stress−strain curves of PDMS and DS films determined through the tensile test (inset: tensile DS sample with a strain value of 300%).

silicone elastomer substrates and hydrolyzed APTES solution containing amine-functional groups was confirmed using attenuated total reflectance Fourier-transform infrared spectroscopy (ATR/FT-IR) and fluorescent labeling.

The conductive graphene-based multilayer electrode was assembled on a modified silicone elastomer surface using electrostatic interactions. Self-assembled electrodes were fabricated based on poly(vinyl alcohol) (PVA), graphene nanoplatelets (GNP), and polystyrene sulfonic acid (PSS; denoted as GL = $[PVA/GNP\text{-}PSS]_n$). To clarify, the newly protonated amine groups in the APTES-modified silicone elastomeric film chemically interacted with the first monolayer of the negatively charged PVA moieties. Then, it was followed by LbL self-assembly to form the GNP-PSS coating via H-bonding.[29−32] The three BL GL electrode was selected and coated owing to its thickness of ∼30 nm and TENG output of ∼4 μA and ∼100 V.[31]

https://doi.org/10.1021/acsomega.3c00008
ACS Omega 2023, 8, 7135−7142

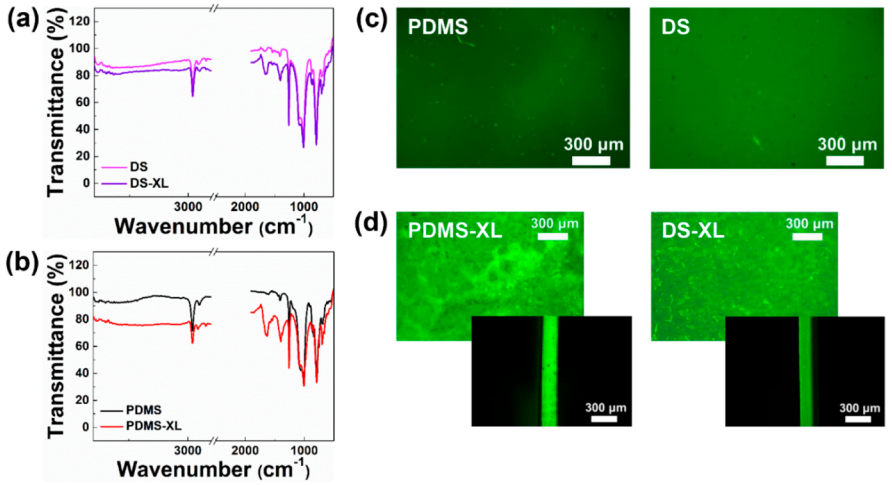

Figure 3. (a) ATR/FT-IR spectra of pristine PDMS and DS, (b) ATR/FT-IR spectra of PDMS and DS films functionalized with APTES, (c) top view of fluorescence labeling of pristine PDMS and DS films, and (d) top view of fluorescence labeling of PDMS and DS films functionalized with APTES (inset: cross sections of functionalized PDMS and DS films).

Water droplet-based TENG (W-TENG) was used to assess the performance of silicone elastomer films with and without chemical XL electrodes. Due to higher surface charge density, the chemically XL silicone elastomer films exhibited higher W-TENG performances than the uncross-linked silicone elastomer films. This result confirmed the screened-out surface charge density for physically attached TM, but chemically XL TMs with electrodes maintained the surface charge density. Furthermore, a strain sensor of the silicone elastomer films with and without chemical XL electrodes was employed by measuring their resistance change ($\Delta R/R_o$) under cyclic stretching and releasing. As a result, the chemical XL electrode silicone elastomers displayed less change in relative resistance to the applied strain than the uncross-linked films. Moreover, the conductive XL-PDMS film demonstrated a significant output performance against repeated mechanical deformations such as twisting, bending, and tapping. Therefore, we presented straightforward, reproducible, and high-performance chemically XL TMs with electrodes as a platform for future wearable electronics.

RESULTS AND DISCUSSION

Preparation and Characterization of Silicone Elastomer Films. Due to its excellent flexibility, softness, optical transparency, and biocompatibility, silicone elastomer film is a promising material for wearable electronics.[23,24] PDMS and DS films were prepared using a straightforward casting procedure, as illustrated in Figure 1. After successfully modifying a silicone elastomer substrate with hydrolyzed APTES solution containing amine-functional groups, it chemically interacted with the first monolayer of the negatively charged PVA moieties. Then, an ultrathin 3 BL $[PVA/GNP\text{-}PSS]_3$ electrode film was fabricated via LbL self-assembly (Figure 1).[29−32]

The peeling tape test was performed to assess the mechanical robustness of the conductive XL-silicone elastomer surface. According to the scheme illustrated in Figure S1a, the conductive XL-PDMS surface was considered for the tape peeling test with cyclic adhesion and detachment operations by the tape. A weight of 450 g was applied to the tape to provide tight adhesion between the coated surface and the strong tape (see the photograph of the tape peeling test in Figure S1b). First, the tape was attached to the conductive XL-PDMS surface, and 450 g of weight was rolled on the sturdy tape while it oscillated. Next, the strong tape was removed from the conductive XL-PDMS surface. This adhesion and peeling process was conducted for 100 cycles. After 100 cycles, a tiny quantity of coated constituents peeled off. So, we performed a single-electrode TENG test to ensure the film withstands its performance by tapping with fingertips. A total of 38 green LEDs were successfully lit up (Figure S1c and Supporting Information Video S1) and exhibited a slight decrease in output voltage (<5%) compared with before the peeling test (Figure 1Sd). This result demonstrated good mechanical stability of the chemically XL electrode silicone elastomer layer.

The surface morphologies of silicone elastomers, PDMS, and DS families were observed using optical microscopy, as shown in Figure 2a. The PDMS film shows a rougher surface than the DS film, whereas the surface of the DS film was smoother and denser. Similarly, the 2D atomic force microscope (AFM) images show the same surface features (Figure 2b). In addition, the average surface roughness values of DS and PDMS films were 0.097 and 0.295 μm, respectively, supporting that the DS coating was relatively smooth, as observed from surface imaging.

The hydrophobicity of each silicone elastomer film was observed by measuring the contact angle under 30% humidity and using a 5 μL droplet of DI water at 27.5 °C for each sample. As shown in Figure 2c, the water contact angles of PDMS and DS were 113.1° and 109.7°, respectively. The PDMS film demonstrated a more hydrophobic surface than the DS film due to its roughness.[17,33] Furthermore, UV−vis light spectral analysis of silicone elastomer films exhibited that the PDMS film was more transparent than the DS film (Figure 2d). Additionally, to demonstrate the silicone elastomer film's stretching and deforming ability, the tensile stress−strain relationship of the film was conducted using the ASTM D412 Type C standard test, as shown in Figure 2e. As the inset demonstrates during elongation, DS film exhibited a higher elongation at break than PDMS film, but the PDMS film exhibited greater strength than the DS film. However, both qualities are important for TENG performance and various applications.[25,26]

https://doi.org/10.1021/acsomega.3c00008
ACS Omega 2023, 8, 7135−7142

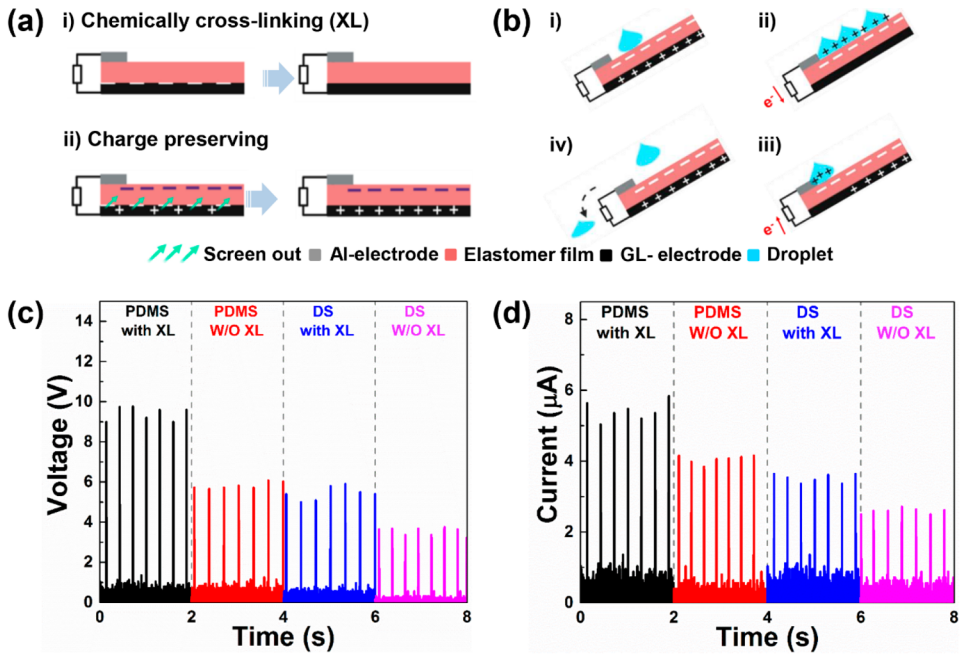

Figure 4. (a) Schematic illustration of charge preserving mechanism of silicone elastomer films with and without chemically cross-linking electrode, (b) TENG power generation mechanism of the water droplet mode (i–iv), and (c,d) output voltage and current of W-TENGs with and without chemical cross-linking of conductive PDMS and DS films.

ATR/FT-IR spectra of PDMS and DS were performed with and without APTES in order to verify the APTES modifications. All characteristic peaks associated with silicone elastomeric films were observed (Figure 3a and b). The common signals appeared at 785 cm^{-1} (Si-CH_3), 1079–1007 cm^{-1} (Si–O–Si), 1259–785 cm^{-1} (Si–CH_3), and 2962 cm^{-1} (CH_3). However, the modified silicone elastomer film exhibited two characteristic peaks attributed to APTES observed at 1629 cm^{-1} (N–H bending) and 3375 cm^{-1} (N–H stretching). Accordingly, it is assumed that the hydrolyzed APTES molecules chemically interacted with the silicone elastomer surface before undergoing a condensation reaction to generate the grafted elastomer surface.[27,34−38]

The modified silicone elastomer surface was subjected to an APTES interaction to fluorescence labeling using rhodamine B. The fluorescence of functionalized surfaces is highly effective and helpful for detecting surface APTES.[24,39] As shown in Figure 3c and d, the modified silicone elastomer strips surpassed the intensity of the pristine silicone strips more than twice, showing a significant concentration of APTES on the modified silicone elastomer surface, evidence of a well-functionalized surface. Additionally, the cross-sectional views show the presence of APTES-treated silicone elastomer surfaces (Figure 3d). Moreover, the UV–vis absorbance spectra of functionalized PDMS and DS films also show an increase in absorbance spectra owing to the presence of APTES (Figure S2a). As a result, these surface alterations facilitated a simple fabrication method by lowering surface degradation and reversion, impeding charge coupling, and enabling simple attachment of ultrathin films to the modified surface.

Performance Analysis of Silicone Elastomer Films. The surface charge density produced on the TM surface dominates the output power of TENGs. However, the surface charge density was screened out by factors such as the abundance of free interfacial electrons and physical adhesion at the electrode–TM contact.[16,18,19] Thus, as shown in Figure 4a,i, these screening issues can be avoided by employing chemical XL electrodes with TMs. Thus, we propose that the surface charge density of TENGs with chemically XL electrodes with silicone elastomer films can be preserved and increase the output power (Figure 4a,ii), which can also completely replace stiff electrodes.[20−23,40]

To demonstrate our concept, a W-TENG device was employed to assess the performance of physical and chemical XL electrode silicone elastomer films.[41] As shown in Figure 4b, water droplets continuously fall on the silicone elastomer surfaces. The contact electrification between the water droplet and the silicone elastomer surface created negative charges and opposite charges on the bottom electrode (Figure 4b,i). First, the induced charges were distributed to the bottom electrode as the water droplet settled on the surface before spreading over it. The droplet then came into contact with the top electrode (Figure 4b,ii). Then, electrons flowed from the top electrode to the bottom electrode until the potential difference was balanced (Figure 4,iii). Once the droplet reached the maximum limit, it contracted and got away from the film. As the water droplet contracted, its spreading area shrank, so opposite charges were induced on the bottom electrode to balance the negative charges on the silicone elastomer surface, resulting in opposite peak signals (Figure 4,iv). Steps i–iv were repeated to generate the AC output power of the W-TENG device. Based on this mechanism, the electrical output performance of silicone elastomer films with and without a chemical XL electrode was conducted under fixed working conditions (i.e., a flow rate of 26 mL/min with tubing cross-section of L/S 16 and contact area of 2 × 3 cm^2).

As shown in Figure 4c and d, the chemically XL electrode silicone elastomer films exhibited higher W-TENG performances in terms of voltage and current than the uncross-linked silicone elastomer films. This increase in output power occurred due to the enhanced surface charge density of

https://doi.org/10.1021/acsomega.3c00008
ACS Omega 2023, 8, 7135−7142

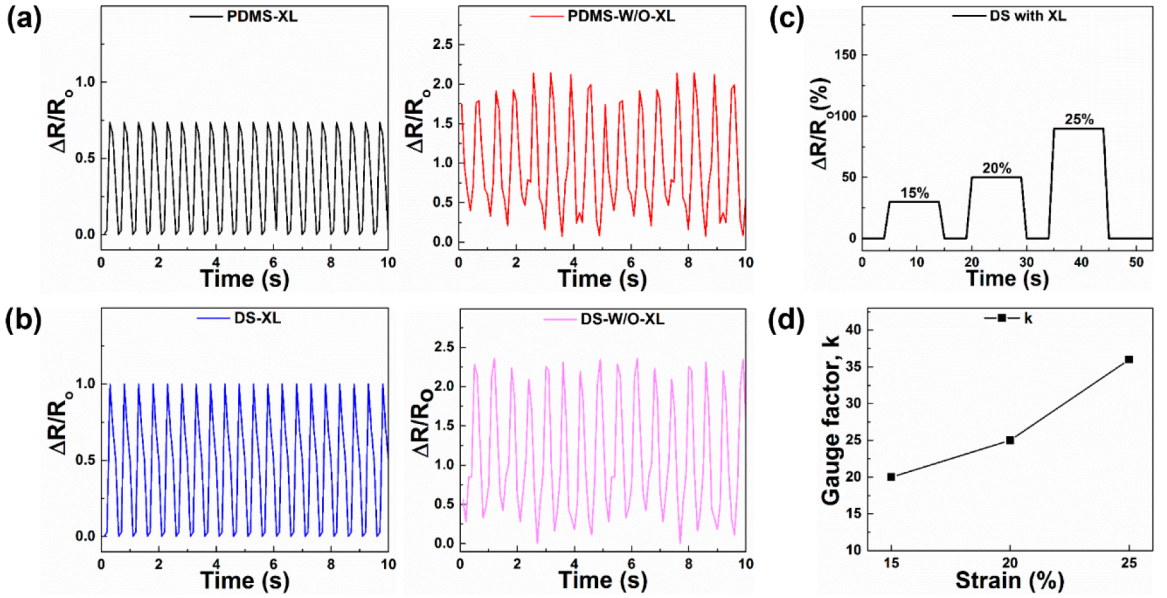

Figure 5. (a,b) The strain sensor shows relative resistance changes during cyclic stretching and releasing with and without cross-linking of PDMS and DS films with the electrode, respectively, and (c,d) relative resistance change and gage factor calculated from the equation of $k\varepsilon = \Delta R/R_o$ for conductive cross-linked DS films under different strains of 15%, 20%, and 25%, respectively.

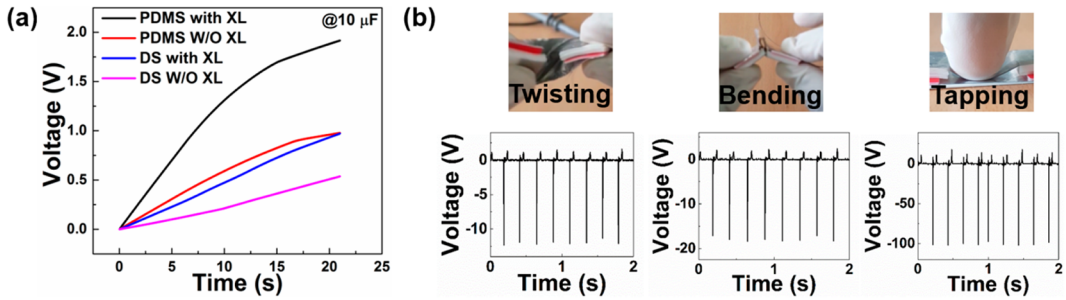

Figure 6. (a) Charging capacitors with and without chemical cross-linking of PDMS and DS films with the electrode and (b) photographs and output voltages of the conductive cross-linked PDMS-based TENG under twisting, bending, and tapping.

chemically XL electrode silicone elastomers. In contrast, the physical adhesion condition created the gap between the TM and electrode interface, yielding surface charge density screened out and lowered results. In addition, the PDMS films showed higher TENG output power than DS films, owing to their surface morphology features such as a higher roughness and contact angle (Figure 2).[17]

Subsequently, the strain sensor performance, $\Delta R/R_o$, with and without chemical XL conductive silicone elastomer films was measured during cyclic stretching and releasing of the index finger. Figure 5a and b show that films without XL display larger $\Delta R/R_o$ values than those with chemical XL. The PDMS and DS films coated without chemical XL demonstrated an exponential increase in $\Delta R/R_o$ due to the gap length created by physical adhesion. Furthermore, because of the lower sheet resistance and higher conductivity (Figure S2b), the conductive XL-PDMS film exhibited a smaller change in $\Delta R/R_o$ than the XL-DS film. Nevertheless, owing to its more significant elongation at break, the conductive XL-DS film was selected for further analysis and attached to various body parts (Figure 2d), exhibiting the improved capacity to withstand the high strain.[42] As a result, significant signal changes were observed under cyclic stimuli of stretching and releasing, except a considerable strain was applied in the film attached to the knee and obtained a relatively higher $\Delta R/R_o$ value (Figure S3 and Supporting Information Video S2).[43]

Furthermore, the effect of varying strains of 15%, 20%, and 25% was evaluated for conductive DS films (Figure 5c). As a result of the strain applied, cracks appeared on the graphene layer, as illustrated in Figure S4. The electrical resistance increased due to the fracture, indicating a partial breakdown of the electrical channels on the graphene layer.[42,44] Figure S4 showed that the size of the crack grew with the increasing strain, leading to a larger $\Delta R/R_o$ at higher strain (Figure 4c). Likewise, the sensitivity of the sensors was compared using the gauge factor, k, calculated from the equation of $k\varepsilon = \Delta R/R_o$, where ε, ΔR, and R_0 represent the applied strain, resistance change with strain, and initial resistance without strain, respectively.[42] At a lower strain of 15%, the DS film showed lower sensitivity ($k = 20$), but at a strain of 25%, it showed higher sensitivity ($k = 39$; Figure 5d). Inspired by this result, we demonstrated this ultrathin conductive XL-DS film as a mechanically responsive strain sensor of a topographic scanner. As a topographic scanner, the XL-DS film was used to detect the cylinders, as shown in a photographic image (Figure S5). As a cylinder passed through the model scanner, the film was bent and warped, resulting in a band of $\Delta R/R_o$ signals (Figure S5a). As more cylinders passed, the $\Delta R/R_o$ signal band and

https://doi.org/10.1021/acsomega.3c00008
ACS Omega 2023, 8, 7135−7142

bending angle also widened (Figure S5b and S5c, and Supporting Information Video S3). Therefore, the chemically XL conductive silicone elastomer films can be used as a flexible wearable strain sensor to detect delicate motions.

To further provide the performance variation between conductive silicone elastomer films with and without chemical XL, we charged a 10 μF capacitor using a single-electrode mode TENG after rectification. The test results exhibited that the charging amount steadily increased initially, then the increasing rate gradually decreased and finally stabilized. As shown in Figure 6a, the chemically XL electrode silicone elastomer film exhibited a higher charging capacity than without chemically XL films. This result demonstrated that the chemically XL TM with the GL electrode helps to maintain the charge density, thereby increasing the efficiency of the nanogenerator.

Finally, we used chemically XL electrode PDMS film to assess TENG performances under various forms of deformation, and Al film (80-μm-thick) was used as a counter TM. Energy harvesting occurred under repeated contact and separation, as shown in Figure 6b, which exhibited 12, 18, and 102 V for twisting, bending, and tapping, respectively. Thus, the chemically XL electrode silicone elastomer film could withstand high strain under repeated contact and separation, which allowed for stable power generation even when the device was highly deformed.

CONCLUSIONS

In summary, the graphene-based electrode with silicone elastomer films was successfully XL by a hydrolyzed APTES solution. The graphene-based multilayer electrode was coated on modified silicone elastomer films using a layer-by-layer assembly method. The ATR/FT-IR spectral analysis and fluorescence labeling confirmed the modified silicone elastomer surface. The W-TENG with a chemically XL electrode of silicone elastomer exhibited an output power of approximately twice that without XL. Furthermore, this chemically XL conductive silicone elastomer film exhibited remarkable stability under repeated mechanical deformation and obtained 12, 18, and 102 V for twisting, bending, and tapping with fingertips and charged capacitors in seconds. In addition, we demonstrated these chemically XL films as a strain sensor to detect subtle movement and exhibited high sensitivity. Therefore, this improved performance and sensitivity of conductive XL silicone elastomer film assembly approach can be an excellent choice for wearable electronics in the future.

EXPERIMENTAL SECTION

Preparation of Silicone Elastomer Films. A 10:1 weight ratio was used to make PDMS elastomer films. First, the mixture was manually mixed for 15 min. Next, the solution was placed in a desiccator for 30 min to degas the trapped air. After, the degassed liquid mixture was cast on the surface of the PET substrate using a mold and the doctor's blade technique, placed in a vacuum desiccator for 30 min at room temperature, and cured at 80 °C in a prepared oven for 4 h to cast the elastomer. After cooling, the cured PDMS elastomer film (0.5-mm-thick) was pulled out of the mold. On the other hand, DS silicone films were prepared by combining part A and part B at a ratio of 1:1 by weight in a mixing container and vigorously mixing for 5 min. The subsequent steps were similar to PDMS film preparation (Figure 1).

Surface Treatment of Silicone Elastomers. The corona-treated elastomer film disk was soaked in 1% v/v hydrolysis APTES solution for 30 min at room temperature with sonication. Then, the elastomer film was washed with DI water and DCM to remove all physically absorbed APTES.

Fluorescent Labeling of Silicone Elastomer Films. A 0.005 mg/mL rhodamine B solution was prepared by dissolving rhodamine B powder in DI water (2 mL). Next, PDMS and DS elastomer strips (with and without XL) were incubated in freshly produced rhodamine B solution for 36 h at room temperature. Over the next 24 h, the strips were soaked six times in 20 mL of DI water.

Characterization. An upright optical microscope (BX40, Olympus Corporation) was used to examine the surface morphology images of the thin films at a magnification of 20×. A UV−vis−NIR spectrometer (DH-2000-BAL, Oceans Optics) was used to investigate the light absorbance and transmittance of each sample. An atomic force microscope (AFM, Anton Paar) was used to determine the roughness of the surface. Water contact angle measurements were performed using a static angle instrument (SDS-TEZD10012, Femtofab, Seongnam, Korea). An FT-IR spectrophotometer (NICOLETiS5, Thermo Scientific) with 32 linear scans and 8 cm^{-1} resolution was used for ATR/FT-IR analysis. Fluorescence microscopy (DX50, Olympus Corporation) was used to examine the cross-sections and surfaces of rhodamine B labeled strips. A universal testing machine (Autograph AGS-X, Shimadzu) was used to measure the mechanical properties of silicone elastomer films. Sheet resistance was measured using a four-point probe (Pro4, Signatone, Gilroy, CA, USA) with a 0.4 mm probe tip diameter and 1.0 mm tip spacing. An oscilloscope (TDS2012B, Tektronix) and a low noise current preamplifier (SR570, Stanford Research Systems) were used to measure electrical output. A peristaltic pump with a Tygon Non-DEHP tubing (L/S series, Masterflex) was used to control the flow rate of water, and resistance changes during stretching and releasing cycles were measured by a 51/2 digit multimeter (34450A, Keysight).

ASSOCIATED CONTENT

Supporting Information

The Supporting Information is available free of charge at https://pubs.acs.org/doi/10.1021/acsomega.3c00008.

Materials; experimental methods for the preparation of conductive electrodes; schematic and performance analysis of the tape-peeling test; UV−vis light absorbance and sheet resistance with the conductivity of conductive XL-silicone elastomer films; strain sensor of resistance change during cyclic stretching and releasing of conductive XL DS film; surface morphology of conductive DS-XL films after different applied strains using optical microscopic; and topographic image of a cylinders scanner with relative resistance change of strain sensors (PDF)

Video S1: Mechanical stability (corresponds to Figure S1c) (MP4)

Video S2: Pointer-finger strain-sensor (corresponds to Figure S3a) (MP4)

Video S3: Mechanical responsive sensor (corresponds to Figure S5c) (MP4)

https://doi.org/10.1021/acsomega.3c00008
ACS Omega 2023, 8, 7135−7142

AUTHOR INFORMATION

Corresponding Authors

Sangmin Lee − *School of Mechanical Engineering, Chung-Ang University, Dongjak-gu, Seoul 06974, Republic of Korea;* orcid.org/0000-0002-6713-4797; Email: slee@cau.ac.kr

Yong Tae Park − *Department of Mechanical Engineering, Myongji University, Yongin, Gyeonggi 17058, Republic of Korea;* orcid.org/0000-0001-9296-6790; Email: ytpark@mju.ac.kr

Authors

Habtamu Gebeyehu Menge − *Department of Mechanical Engineering, Myongji University, Yongin, Gyeonggi 17058, Republic of Korea; School of Mechanical Engineering, Chung-Ang University, Dongjak-gu, Seoul 06974, Republic of Korea;* orcid.org/0000-0002-1023-0147

Min Woo Kim − *Department of Mechanical Engineering, Myongji University, Yongin, Gyeonggi 17058, Republic of Korea*

Complete contact information is available at: https://pubs.acs.org/10.1021/acsomega.3c00008

Author Contributions

The manuscript was written through the contributions of all authors. All authors approved the final version of the manuscript.

Notes

The authors declare no competing financial interest.

ACKNOWLEDGMENTS

This work was supported by the National Research Foundation of Korea (NRF) grant funded by the Korean government (MSIP; Nos. 2022R1A2C2006081 and 2021R1A4A3030268) Chung-Ang University research grant in 2021 and 2022 research fund of Myongji University.

REFERENCES

(1) Atzori, L.; Iera, A.; Morabito, G. The internet of things: A survey. *Comput. Netw.* **2010**, *54* (15), 2787−2805.

(2) Wang, Z. L. Triboelectric nanogenerators as new energy technology for self-powered systems and as active mechanical and chemical sensors. *ACS Nano* **2013**, *7* (11), 9533−9557.

(3) Fan, F.-R.; Tian, Z.-Q.; Lin Wang, Z. Flexible triboelectric generator. *Nano Energy* **2012**, *1* (2), 328−334.

(4) Wang, Z. L.; Chen, J.; Lin, L. Progress in triboelectric nanogenerators as a new energy technology and self-powered sensors. *Energy Env. Sci.* **2015**, *8* (8), 2250−2282.

(5) Zhu, G.; Peng, B.; Chen, J.; Jing, Q.; Lin Wang, Z. Triboelectric nanogenerators as a new energy technology: from fundamentals, devices, to applications. *Nano Energy* **2015**, *14*, 126−138.

(6) Fan, F.-R.; Lin, L.; Zhu, G.; Wu, W.; Zhang, R.; Wang, Z. L. Transparent triboelectric nanogenerators and self-powered pressure sensors based on micropatterned plastic films. *Nano Lett.* **2012**, *12* (6), 3109−3114.

(7) Yang, Y.; Zhang, H.; Lin, Z.-H.; Zhou, Y. S.; Jing, Q.; Su, Y.; Yang, J.; Chen, J.; Hu, C.; Wang, Z. L. Human skin-based triboelectric nanogenerators for harvesting biomechanical energy and as self-powered active tactile sensor system. *ACS Nano* **2013**, *7* (10), 9213−9222.

(8) Liu, C.; Li, J.; Che, L.; Chen, S.; Wang, Z.; Zhou, X. Toward large-scale fabrication of triboelectric nanogenerator (TENG) with silk-fibroin patches film via spray-coating process. *Nano Energy* **2017**, *41*, 359−366.

(9) Jin, S.; Wang, Y.; Motlag, M.; Gao, S.; Xu, J.; Nian, Q.; Wu, W.; Cheng, G. J. Large-area direct laser-shock imprinting of a 3D biomimic hierarchical metal surface for triboelectric nanogenerators. *Adv. Mater.* **2018**, *30* (11), 1705840.

(10) Salauddin, M.; Rana, S. M.; Sharifuzzaman, M.; Rahman, M. T.; Park, C.; Cho, H.; Maharjan, P.; Bhatta, T.; Park, J. Y. A novel MXene/Ecoflex nanocomposite-coated fabric as a highly negative and stable friction layer for high-output triboelectric nanogenerators. *Adv. Energy Mater.* **2021**, *11* (1), 2002832.

(11) Liu, G.; Gao, Y.; Xu, S.; Bu, T.; Xie, Y.; Xu, C.; Zhou, H.; Qi, Y.; Zhang, C. One-stop fabrication of triboelectric nanogenerator based on 3D printing. *EcoMat* **2021**, *3* (5), 12130.

(12) Walden, R.; Kumar, C.; Mulvihill, D. M.; Pillai, S. C. Opportunities and challenges in triboelectric nanogenerator (TENG) based sustainable energy generation technologies: a mini-review. *Chem. Eng.* **2022**, *9*, 100237.

(13) Yu, Y.; Wang, X. Chemical modification of polymer surfaces for advanced triboelectric nanogenerator development. *Extreme Mech. Lett.* **2016**, *9*, 514−530.

(14) Liu, W.; Wang, Z.; Hu, C. Advanced designs for output improvement of triboelectric nanogenerator system. *Mater. Today* **2021**, *45*, 93−119.

(15) Ryu, H.; Yoon, H. J.; Kim, S. W. Hybrid energy harvesters: toward sustainable energy harvesting. *Adv. Mater.* **2019**, *31* (34), 1802898.

(16) Menge, H. G.; Huynh, N. D.; Cho, C.; Choi, D.; Park, Y. T. Designable functional polymer nanocomposites via layer-by-layer assembly for highly deformable power-boosted triboelectric nanogenerators. *Comp. part B* **2022**, *230*, 109513.

(17) Menge, H. G.; Kim, J. O.; Park, Y. T. Enhanced triboelectric performance of modified PDMS nanocomposite multilayered nanogenerators. *Materials* **2020**, *13* (18), 4156.

(18) Cui, N.; Gu, L.; Lei, Y.; Liu, J.; Qin, Y.; Ma, X.-H.; Hao, Y.; Wang, Z. L. Dynamic behavior of the triboelectric charges and structural optimization of the friction layer for a triboelectric nanogenerator. *ACS Nano* **2016**, *10* (6), 6131−6138.

(19) Wu, C.; Kim, T. W.; Choi, H. Y. Reduced graphene-oxide acting as electron-trapping sites in the friction layer for giant triboelectric enhancement. *Nano Energy* **2017**, *32*, 542−550.

(20) Kim, D. H.; Rogers, J. A. Stretchable electronics: materials strategies and devices. *Adv. Mater.* **2008**, *20* (24), 4887−4892.

(21) Kim, Y.; Zhu, J.; Yeom, B.; Di Prima, M.; Su, X.; Kim, J.-G.; Yoo, S. J.; Uher, C.; Kotov, N. A. Stretchable nanoparticle conductors with self-organized conductive pathways. *Nature Lett.* **2013**, *500* (7460), 59−63.

(22) Wang, C.; Pan, C.; Wang, Z. L. Electronic skin for closed-loop systems. *ACS Nnao* **2019**, *13* (11), 12287−12293.

(23) Lee, S.; Song, Y.; Ko, Y.; Ko, Y.; Ko, J.; Kwon, C. H.; Huh, J.; Kim, S.-W.; Yeom, B.; Cho, J. A Metal-like conductive elastomer with a hierarchical wrinkled structure. *Adv. Mater.* **2020**, *32* (7), 1906460.

(24) Zhang, J.; Chen, Y.; Brook, M. A. Facile functionalization of PDMS elastomer surfaces using thiol-ene click chemistry. *Langmuir* **2013**, *29* (40), 12432−12442.

(25) Park, S.; Mondal, K.; Treadway, R. M.; Kumar, V.; Ma, S.; Holbery, J. D.; Dickey, M. D. Silicones for stretchable and durable soft devices: Beyond Sylgard-184. *ACS Appl. Mater. Interfaces* **2018**, *10* (13), 11261−11268.

(26) Zhu, Z.; Chen, P.; Liu, K.; Escobedo, C. A versatile bonding method for PDMS and SU-8 and its application towards a multifunctional microfluidic device. *Micromachines* **2016**, *7* (12), 230.

(27) Majoul, N.; Aouida, S.; Bessaïs, B. Progress of porous silicon APTES-functionalization by FTIR investigations. *Appl. Mater. Sci.* **2015**, *331*, 388−391.

(28) Magalhães, S.; Alves, L.; Medronho, B.; Fonseca, A. C.; Romano, A.; Coelho, J. F. J.; Norgren, M. Brief overview on bio-based adhesives and sealants. *Polymers* **2019**, *11* (10), 1685.

(29) Mun, S. C.; Park, J. J.; Park, Y. T.; Kim, D. Y.; Lee, S. W.; Cobos, M.; Ye, S. J.; Macosko, C. W.; Ok Park, O High electrical conductivity and oxygen barrier property of polymer-stabilized graphene thin films. *Carbon* **2017**, *125*, 492−499.

(30) Menge, H. G.; Huynh, N. D.; Hwang, H. J.; Han, S.; Choi, D.; Park, Y. T. Designable skin-like triboelectric nanogenerators using layer-by-layer self-assembled polymeric nanocomposites. *ACS Energy Lett.* **2021**, *6* (7), 2451−2459.
(31) Chung, I. J.; Kim, W.; Jang, W.; Park, H.-W.; Sohn, A.; Chung, K.-B.; Kim, D.-W.; Choi, D.; Park, Y. T. Layer-by-layer assembled graphene multilayers on multidimensional surfaces for highly durable, scalable, and wearable triboelectric nanogenerators. *J. Mater. Chem. A* **2018**, *6* (7), 3108−3115.
(32) Menge, H. G.; Jo, S. H.; Park, Y. T. Layer-by-Layer Self-Assembled Thin Films for Triboelectric Energy Harvesting under Harsh Conditions. *ACS Appl. Electron. Mater.* **2021**, *3* (12), 5475−5482.
(33) Cassie, A. B. D.; Baxter, S. Wettability of porous surfaces. *J. Chem. Soc. Faraday Trans.* **1944**, *40*, 546−551.
(34) Le, T.-N.; Lee, C.-K. Surface functionalization of poly (N-vinylpyrrolidone) onto poly (dimethylsiloxane) for anti-biofilm application. *Biochem. Biotechnol.* **2020**, *191* (1), 29−44.
(35) Stafie, N.; Stamatialis, D.F.; Wessling, M. Effect of PDMS cross-linking degree on the permeation performance of PAN/PDMS composite nanofiltration membranes. *Sep. Purif. Technol.* **2005**, *45* (3), 220−231.
(36) Nayak, N.; Huertas, R.; Crespo, J. G.; Portugal, C. A.M. Surface modification of alumina monolithic columns with 3-aminopropyltetraethoxysilane (APTES) for protein attachment. *Sep. Purif. Technol.* **2019**, *229*, 115674.
(37) Howarter, J. A.; Youngblood, J. P. Optimization of silica silanization by 3-aminopropyltriethoxysilane. *Langmuir* **2006**, *22* (26), 11142−11147.
(38) Sunkara, V.; Cho, Y.-K. Investigation on the mechanism of aminosilane-mediated bonding of thermoplastics and poly (dimethylsiloxane). *ACS Appl. Mater. Interfaces* **2012**, *4* (12), 6537−6544.
(39) Rusen, E.; Mocanu, A.; Diacon, A.; Marculescu, B. Fluorescence enhancement of rhodamine B in the presence of photonic crystal heterostructures. *Phys. Chem.* **2011**, *115* (30), 14947−14953.
(40) Moon, G. D.; Lim, G.-H.; Song, J. H.; Shin, M.; Yu, T.; Lim, B.; Jeong, U. Highly stretchable patterned gold electrodes made of Au nanosheets. *Adv. Mater.* **2013**, *25* (19), 2707−2712.
(41) Ye, C.; Liu, D.; Peng, X.; Jiang, Y.; Cheng, R.; Ning, C.; Sheng, F.; Zhang, Y.; Dong, K.; Wang, Z. L. A Hydrophobic Self-Repairing Power Textile for Effective Water Droplet Energy Harvesting. *ACS Nano* **2021**, *15* (11), 18172−18181.
(42) Lee, S. W.; Park, B. J.; Park, S. C.; Mun, S. C.; Park, Y. T.; Liao, K.; Seo, T. S.; Hyun, W. J.; Park, O. O. Enhanced sensitivity of patterned graphene strain sensors used for monitoring subtle human body motions. *ACS Appl. Mater. Interfaces* **2017**, *9* (12), 11176−11183.
(43) An, H.; Habib, T.; Shah, S.; Gao, H.; Radovic, M.; Green, M. J.; Lutkenhaus, J. L. Surface-agnostic highly stretchable and bendable conductive MXene multilayers. *Sci. Adv.* **2018**, *4* (3), 0118.
(44) Li, X.; Zhang, R.; Yu, W.; Wang, K.; Wei, J.; Wu, D.; Cao, A.; Li, Z.; Cheng, Y.; Zheng, Q.; Ruoff, R. S.; Zhu, H. Stretchable and highly sensitive graphene-on-polymer strain sensors. *Sci. Rep.* **2012**, *2* (1), 1−6.

https://doi.org/10.1021/acsomega.3c00008
ACS Omega 2023, 8, 7135−7142